HSPC117 Is the Essential Subunit of a Human tRNA Splicing Ligase Complex

Johannes Popow, *et al.*

Science **331**, 760 (2011);
DOI: 10.1126/science.1197847

We used NMR spectroscopy to interrogate binding between MyTH4 and CEN2. A 21-residue synthetic peptide corresponding to CEN2 was confirmed to bind to MFS using the transferred nuclear Overhauser effect (NOE) technique (Fig. 3A and fig. S15). We determined the structure of the MFS-bound CEN2 with the use of transferred NOE-derived distance restraints (Fig. 3B and table S2). A seven-residue fragment (372 to 378) of CEN2 adopts a defined conformation, with the aromatic ring of W374 sandwiched by P373, L372, and L377, forming a hydrophobic cluster. The opposite face of this hydrophobic cluster contains five negatively charged residues (Fig. 3C). The CEN2 NMR structure was docked to the MyTH4 domain using the program HADDOCK (*21*). The final docked structure reveals a good surface match between CEN2 and MyTH4, and the CEN2 peptide fits reasonably well with the unexplained electron densities observed in MyTH4 (Fig. 3D). Together with the cellular imaging data (fig. S3), we conclude that CEN2 contributes to the overall binding between MFS and CEN.

A total of 19 missense mutations involving 17 amino acids within MYO7A-MFS have been documented in Usher syndrome patients (fig. S1). The distribution of the 17 missense variants is mapped onto the structure of MFS (Fig. 4; truncation/deletion mutations are not discussed here as these can be interpreted as null mutations). Among the 17 mutation sites, 7 are in MyTH4, 9 in FERM, and 1 in SH3 (Fig. 4B). These 17 MYO7A-MFS variants can be divided into four classes (fig. S16): The first class of the mutations occurs in the folding core of the MyTH4 domain [Ile^{1045}→Thr^{1045} (I1045T), R1168P/W, E1170K, P1183T, R1240Q/W, and P1244R] or the FERM domain (A1288P in F1 and L1484F in F3) (Fig. 4 and fig. S16A). The disease-causing mutations in this category are likely to have a deleterious impact on the folding of the MyTH4-FERM supramodule. The mutations in the second class (G1218K in MyTH4; E1327K, A1340P, and E1349K in F1; A1492V in F3) may not affect the structure of the individual domains but instead are likely to interfere with the interdomain interactions or the interaction between MYO7A and Sans, as these residues are situated in the interface between the domains, as well as in the interface between MFS and Sans CEN (Fig. 4 and fig. S16B). For example, E1349 is intimately involved in binding to Sans CEN1; the E1349K-MFS mutation weakens its Sans binding by ~20-fold (fig. S2D). The third class of mutants involves the conserved R1343 in F1 and R1602 in F3. Both of these residues are solvent-exposed and not expected to play obvious structural roles in MFS folding or in Sans binding, but they may affect interactions between MYO7A-MFS and its other partners (Fig. 4 and fig. S16C). The fourth class of mutations (T1566M and A1628S) cannot be interpreted by the MFS/CEN structure.

Structure-based sequence analysis indicates that the supramodular nature is probably a general property of other MyTH4-FERM tandems (fig. S10). In the MYO7A-MFS, α9, α10, and the α9/α10 loop of MyTH4 form the MyTH4/FERM interface (fig. S5B). The α9/α10 loop and α10 contain a conserved R-X-X-X-P-X-(X)-X-E motif in all MyTH4 domains (fig. S11). The Arg and Glu residues in this motif form a salt bridge to define the orientation of α9 and α10, and the Pro residue (P1244) facilitates the formation of the turn structure in the α9/α10 loop (Fig. 4A). Mutations of Arg or Pro residue in this signature motif of either of the MYO7A MyTH4-FERM tandems cause deaf-blindness in humans (fig. S10). The supramodular structure of MYO7A-MFS also correlates well with the observation that MyTH4 domains invariably coexist with FERM domains in MyTH4-containing proteins. Finally, sequence-alignment analysis further predicts that the majority of the disease-causing mutations in the second MYO7A MyTH4-FERM tandem would either disrupt the folding of the domains or cripple the inter-MyTH4-FERM interface (fig. S10). The MYO7A-MFS structure not only provides mechanistic explanations to currently known disease-causing mutations in the MYO7A MyTH4-FERM tandems, but it will also be valuable in understanding functions of other MyTH4-FERM containing myosins.

References and Notes

1. S. Riazuddin *et al.*, *Hum. Mutat.* **29**, 502 (2008).
2. T. Jaïjo *et al.*, *J. Med. Genet.* **44**, e71 (2007).
3. J. Reiners, U. Wolfrum, *Adv. Exp. Med. Biol.* **572**, 349 (2006).
4. A. El-Amraoui, C. Petit, *J. Cell Sci.* **118**, 4593 (2005).
5. Z. M. Ahmed, S. Riazuddin, S. Riazuddin, E. R. Wilcox, *Clin. Genet.* **63**, 431 (2003).
6. X. M. Ouyang *et al.*, *Hum. Genet.* **116**, 292 (2005).
7. A. Adato *et al.*, *Hum. Mol. Genet.* **14**, 347 (2005).
8. B. Boëda *et al.*, *EMBO J.* **21**, 6689 (2002).
9. J. Siemens *et al.*, *Proc. Natl. Acad. Sci. U.S.A.* **99**, 14946 (2002).
10. G. Lefèvre *et al.*, *Development* **135**, 1427 (2008).
11. M. Schwander, B. Kachar, U. Müller, *J. Cell Biol.* **190**, 9 (2010).
12. A. Wang *et al.*, *Science* **280**, 1447 (1998).
13. F. J. Probst *et al.*, *Science* **280**, 1444 (1998).
14. D. Well *et al.*, *Nature* **374**, 60 (1995).
15. T. Self *et al.*, *Development* **125**, 557 (1998).
16. M. Schwander *et al.*, *J. Neurosci.* **29**, 15810 (2009).
17. D. Weil *et al.*, *Hum. Mol. Genet.* **12**, 463 (2003).
18. Materials and methods are available as supporting material on *Science* Online.
19. U. Tepass, *Curr. Opin. Genet. Dev.* **19**, 357 (2009).
20. Single-letter abbreviations for the amino acid residues are as follows: A, Ala; C, Cys; D, Asp; E, Glu; F, Phe; G, Gly; H, His; I, Ile; K, Lys; L, Leu; M, Met; N, Asn; P, Pro; Q, Gln; R, Arg; S, Ser; T, Thr; V, Val; W, Trp; Y, Tyr; and X, any amino acid.
21. C. Dominguez, R. Boelens, A. M. Bonvin, *J. Am. Chem. Soc.* **125**, 1731 (2003).

22. We thank T. Friediman for providing the mouse MYO7A cDNA construct, J. Yu and Y. Shang for the help in crystallography, Y. Zhao for the in-house x-ray diffractor, the BL17U1 of the Shanghai Synchrotron Radiation Facility for the beamline time, and A. Zhang for reading the manuscript. This work was supported by grants from the Research Grant Council of Hong Kong to M.Z. (663808, 664009, 663610, CA07/08.SC01, SEG_HKUST06, and AoE/B-15/01-II). The atomic coordinates and structure factors of the complex structure have been deposited in the Protein Data Bank under the accession code 3PVL. The superimposed final 10 NMR structures of the CEN2 peptide have been deposited in the Protein Data Bank under the accession code 2L7T.

Supporting Online Material

www.sciencemag.org/cgi/content/full/331/6018/757/DC1
Materials and Methods
Figs. S1 to S16
Tables S1 and S2
References

8 October 2010; accepted 3 January 2011
10.1126/science.1198848

HSPC117 Is the Essential Subunit of a Human tRNA Splicing Ligase Complex

Johannes Popow,[1]* Markus Englert,[2]* Stefan Weitzer,[1] Alexander Schleiffer,[3] Beata Mierzwa,[1] Karl Mechtler,[4] Simon Trowitzsch,[5]† Cindy L. Will,[5] Reinhard Lührmann,[5] Dieter Söll,[2,6]‡ Javier Martinez[1]‡

Splicing of mammalian precursor transfer RNA (tRNA) molecules involves two enzymatic steps. First, intron removal by the tRNA splicing endonuclease generates separate 5′ and 3′ exons. In animals, the second step predominantly entails direct exon ligation by an elusive RNA ligase. Using activity-guided purification of tRNA ligase from HeLa cell extracts, we identified HSPC117, a member of the UPF0027 (RtcB) family, as the essential subunit of a tRNA ligase complex. RNA interference–mediated depletion of HSPC117 inhibited maturation of intron-containing pre-tRNA both in vitro and in living cells. The high sequence conservation of HSPC117/RtcB proteins is suggestive of RNA ligase roles of this protein family in various organisms.

Transfer RNAs (tRNAs) are essential adaptor molecules in the translation of the genetic transcript into proteins. During their post-transcriptional maturation (*1*), intron-containing tRNA precursor transcripts (pre-tRNAs) undergo splicing, which is accomplished by a specialized endonuclease that excises the intron (*2*, *3*) and a ligase that joins the resulting exon halves (fig. S1A). Although introns within pre-tRNA transcripts have been detected in all domains of life,

[1]Institute of Molecular Biotechnology of the Austrian Academy of Sciences (IMBA), A-1030 Vienna, Austria. [2]Department of Molecular Biophysics and Biochemistry, Yale University, New Haven, CT 06520, USA. [3]Bioinformatics Department, Research Institute of Molecular Pathology (IMP)–IMBA, A-1030 Vienna, Austria. [4]Protein Chemistry Department, Research Institute of Molecular Pathology (IMP)–IMBA, A-1030 Vienna, Austria. [5]Department of Cellular Biochemistry, Max Planck Institute for Biophysical Chemistry, 37077 Göttingen, Germany. [6]Department of Chemistry, Yale University, New Haven, CT 06520, USA.

*These authors contributed equally to this work.
†Present address: European Molecular Biology Laboratory, Grenoble Outstation, and Unit of Virus Host Cell Interactions, UMI3265, Grenoble Cedex 9, France.
‡To whom correspondence should be addressed. E-mail: javier.martinez@imba.oeaw.ac.at (J.M.); dieter.soll@yale.edu (D.S.)

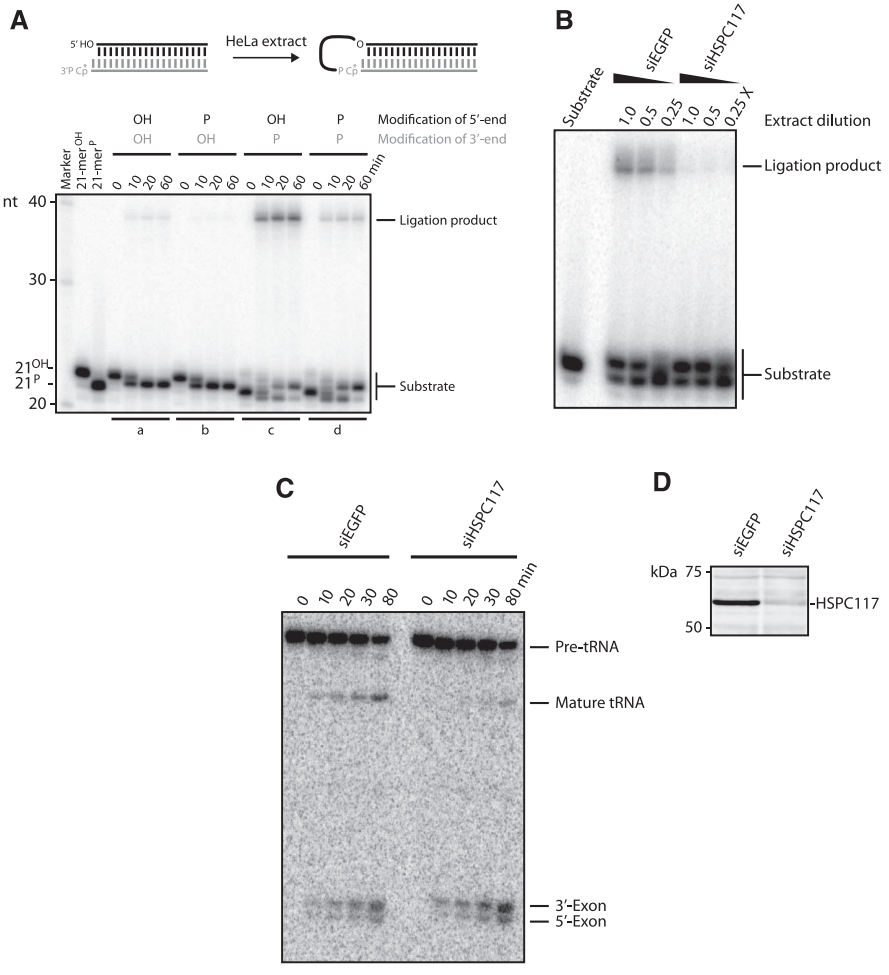

Fig. 1. Identification of the RNA>p ligase HSPC117. (**A**) (Upper panel) Scheme illustrating dsRNA interstrand ligation. 5′-OH, 3′-P RNA oligonucleotides (depicted in gray; asterisk marks position of radiolabel) were incubated with (lanes a and b) or without (lanes c and d) alkaline phosphatase and annealed to complementary RNA strands (depicted in black) incubated with (lanes a and c) or without (lanes b and d) T4 Pnkp and ATP. The obtained RNA duplexes were used as substrates for interstrand ligation in HeLa cell extracts (lower panel). (**B** and **C**) Dilution series of protein extracts prepared from cells transfected with small interfering RNAs (siRNAs) targeting HSPC117 and enhanced green fluorescent protein (EGFP) as a control were assayed for interstrand ligation (B) and tRNA maturation (C). (**D**) Depletion of HSPC117 was confirmed by Western blot.

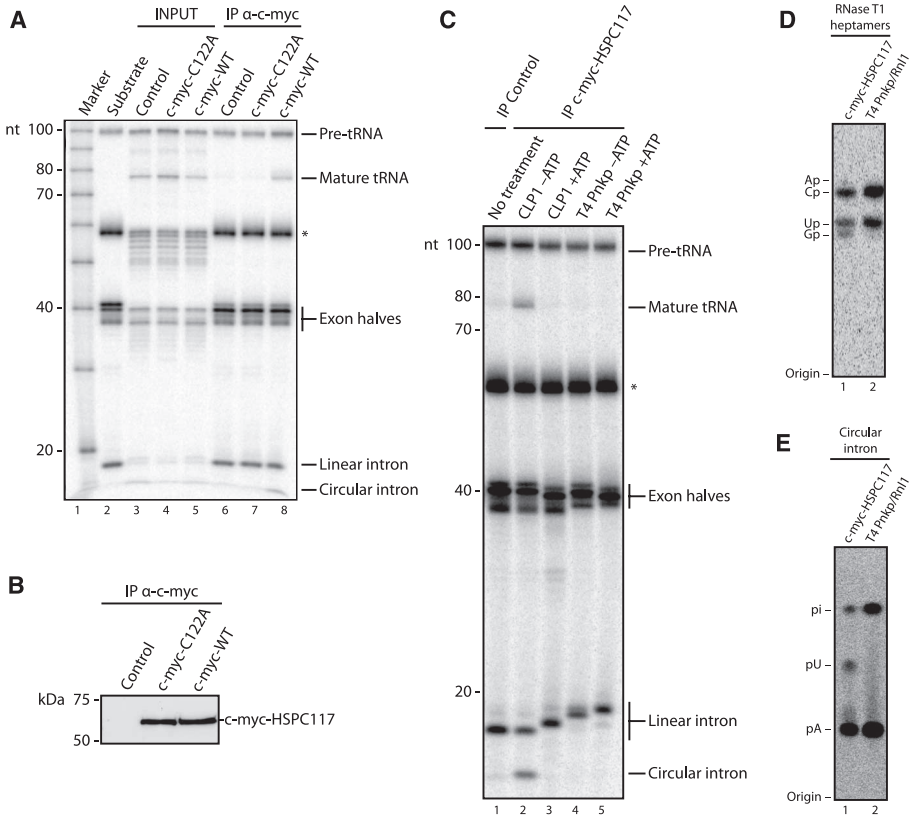

Fig. 2. Affinity purification of c-myc–HSPC117 from stably transfected HeLa cell lines yields an RNA>p ligase. (**A**) Immunoprecipitates (IPs) of wild-type (WT) or C122A c-myc–HSPC117 were incubated with tRNA exon halves. An IP prepared from a non-expressing clone was used as negative control. Asterisks denote unrelated bands. (**B**) Detection of WT and mutant c-myc–HSPC117 in IPs by Western blot. (**C**) tRNA exon halves were incubated with recombinant CLP1 or T4 Pnkp in the presence or absence of ATP and used as a substrate for ligation with c-myc–HSPC117. (**D**) RNase T1 fragments derived from [α-^{32}P]UTP-radiolabeled mature tRNA generated either by T4 Pnkp/Rnl1 or affinity-purified c-myc–HSPC117 were resolved by denaturing gel electrophoresis. RNA heptamers were isolated from the gel, digested with RNase T2, and analyzed by thin-layer chromatography (TLC). (**E**) Circular, [α-^{32}P]ATP-radiolabeled intron generated either by T4 Pnkp/Rnl1 or affinity-purified c-myc–HSPC117 was isolated from gels, digested with nuclease P1, and analyzed by TLC.

the splicing machinery diverged at the ligation step during evolution (*4*). In fungi and plants, multifunctional proteins (*5*–*7*) homologous to bacteriophage T4 RNA ligase 1 (T4 Rnl1) (*8*) prepare the exon termini by the action of cyclic phosphodiesterase and polynucleotide kinase activities before catalyzing the actual ligation (fig. S1A, upper branch) (*9*, *10*). In contrast, the animal and archaeal clades ligate tRNA exons by directly joining the 2′,3′-cyclic phosphate (RNA>p) and 5′-OH termini left after cleavage, leading to incorporation of the precursor-derived 2′,3′-cyclic phosphate into the splice junction (fig. S1A, lower branch) (*11*–*14*). No RNA>p ligase has been identified since the direct tRNA splicing pathway was initially postulated.

By serendipity, it was discovered that 3′-phosphorylated (3′-P), 5′-OH double-stranded RNA (dsRNA) molecules become covalently linked upon incubation with human cell extracts (Fig. 1A, upper panel, and fig. S1, B and C) (*15*, *16*) after their conversion into 2′,3′-cyclic phosphate–terminated dsRNA (*11*, *17*). Removal of the 3′-phosphate, phosphorylation of the 5′-OH, or a combination of both inhibited interstrand ligation (Fig. 1A, lower panel). Therefore, we decided to use 3′-P dsRNA as a stable surrogate substrate for human tRNA ligase. By monitoring interstrand ligation, we were able to follow RNA>p ligase activity along three chromatographic purification steps (fig. S1, D and E) and used the resulting RNA>p ligase–enriched MonoQ fraction to identify 91 proteins by tryptic digestion and tandem mass spectrometry (MS) (table S1). HSPC117/C22ORF28, a member of the uncharacterized protein family UPF0027 (*18*), appeared to be of particular interest, as it is the human homolog of the bacterial and archaeal *RtcB* gene, which, together with RtcA, the RNA 3′-P terminal cyclase, resides within a σ54-regulated operon in *Escherichia coli* (*19*). As a consequence, HSPC117/RtcB proteins have been predicted to function in RNA processing or modification (*20*). Both RNA>p ligase activity and the UPF0027 protein family are not detectable in plant and fungal model organisms (e.g., *Arabidopsis thaliana* or *Saccharomyces cerevisiae*) (*4*, *18*), suggesting a link between HSPC117 and direct RNA ligation.

Depleting HSPC117 by RNA interference (RNAi) abolished interstrand ligation (Fig. 1B and fig. S2) and impaired processing of pre-tRNA transcripts into mature tRNA in cell extracts,

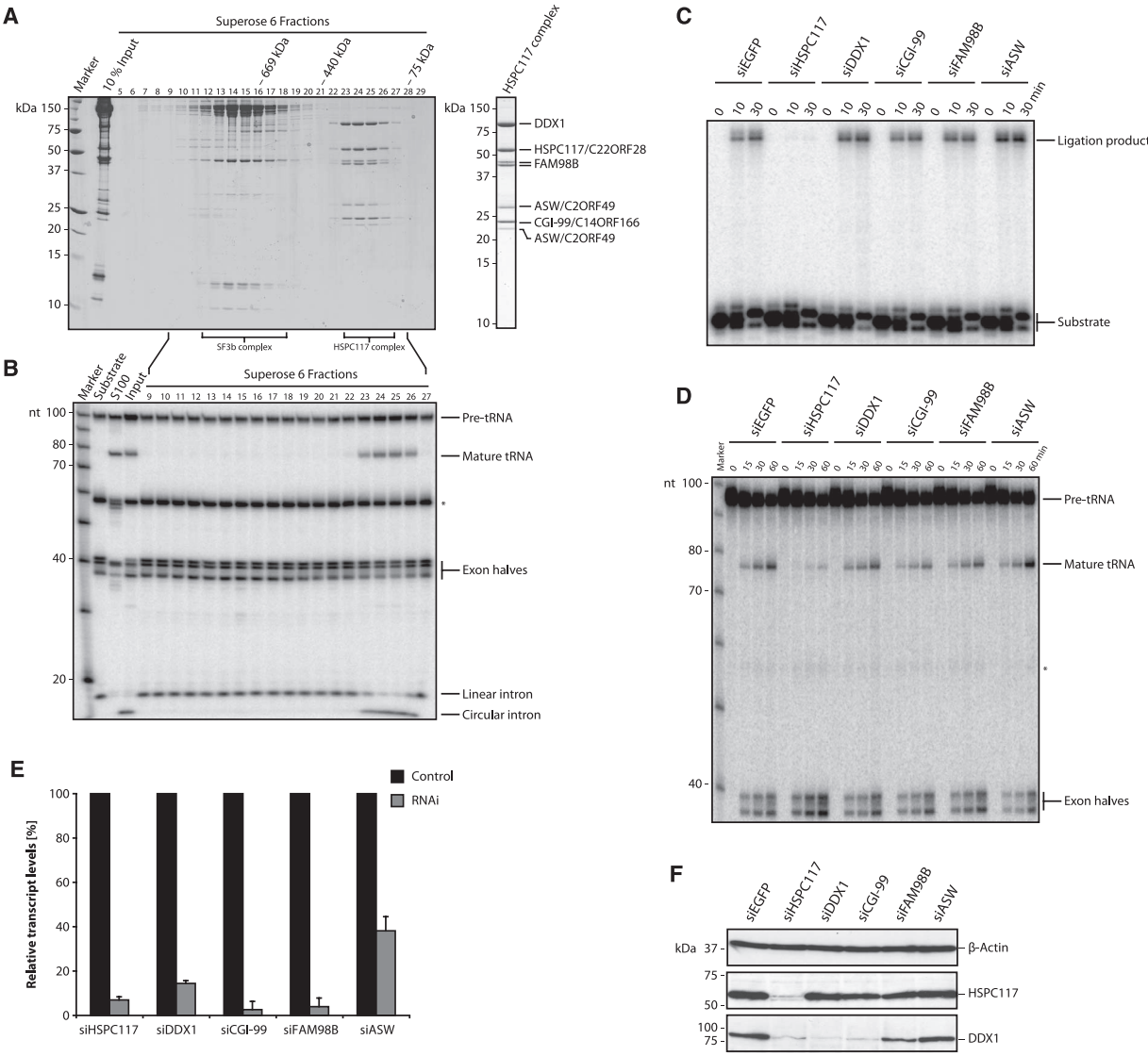

Fig. 3. An active RNA>p ligase complex is co-selected with SF3b monoclonal antibodies. (**A**) Size exclusion chromatography of SF3b and HSPC117 complexes after affinity co-selection. Fractions were analyzed by SDS–polyacrylamide gel electrophoresis. (**B**) tRNA exon half ligation assay of eluted fractions. Asterisks denote unrelated bands. (**C** and **D**) Extracts prepared from cells depleted of HSPC117, DDX1, CGI-99, FAM98B, ASW, and EGFP as a control were assayed for interstrand ligation (C) and tRNA maturation (D). (**E**) Confirmation of the depletion of *HSPC117*, *DDX1*, *CGI-99*, *FAM98B*, and *ASW* mRNAs by quantitative polymerase chain reaction (PCR). Results are depicted as means ± SD of triplicate PCR reactions. (**F**) Western blot for HSPC117, DDX1, FAM98B, and β-actin as a loading control.

leading to a concomitant accumulation of exon halves. These findings are consistent with a role in the ligation of tRNA exons (Fig. 1, C and D).

Assuming that mutation of a strictly conserved cysteine residue (fig. S3) predicted to be involved in metal ion coordination in RtcB proteins (*21*, *22*) would render the enzyme inactive, we created clonal cell lines expressing wild-type c-myc–HSPC117 and the point mutant C122A ($Cys^{122} \rightarrow Ala^{122}$). Affinity purification of c-myc–HSPC117 yielded an immunoprecipitate ligating tRNA exon halves (Fig. 2A, lane 8). In contrast, the point mutant c-myc–HSPC117 C122A was inactive as a tRNA ligase (Fig. 2A, lane 7) in immunoprecipitates containing equal amounts of wild-type and C122A mutant c-myc–HSPC117 (Fig. 2B and fig. S4).

RNA>p ligase requires a 5′-OH at the termini of its substrates. Accordingly, no ligase activity could be detected in c-myc–HSPC117 immunoprecipitates when tRNA exon halves were phosphorylated with the recombinant 5′-OH RNA kinase CLP1 (*23*) (Fig. 2C, compare lanes 2 and 3). Removing the 2′,3′-cyclic phosphate of the tRNA 5′ exon with bacteriophage T4 polynucleotide kinase (T4 Pnkp) abolished ligase activity of c-myc–HSPC117 immunoprecipitates (Fig. 2C, lanes 4 and 5). Thus, ligation by HSPC117 is dependent on 5′-OH (see also Fig. 1A) and 2′,3′-cyclic phosphate.

To test whether ligation by HSPC117 results in incorporation of the precursor-derived 2′,3′-cyclic phosphate into mature tRNA, we performed a nearest-neighbor analysis of the splice junction phosphate (*12*, *14*) (fig. S1A, lower branch, and fig. S5). tRNA exon halves with a radiolabeled 2′,3′-cyclic phosphate at the terminus of the 5′-exon half were prepared from [α-^{32}P] uridine triphosphate (UTP)–radiolabeled pre-tRNA (fig. S5A) and were ligated either with c-myc–HSPC117 immunoprecipitate or with a mixture of T4 Pnkp and T4 Rnl1 as a negative control. The precursor-derived 2′,3′-terminal phosphate, liberated as guanosine 3′-monophosphate (Gp) upon digestion of the splice junction of mature tRNA with ribonuclease (RNase) T2, was retained only upon ligation with c-myc–HSPC117 (Fig. 2D, lane 1) but not with T4 Pnkp/T4 Rnl1 (Fig. 2D, lane 2). A similar nearest-neighbor analysis was also carried out with [α-^{32}P]adenosine triphosphate (ATP)–radiolabeled linear intron after its conversion to circularized intron by c-myc–HSPC117 immunoprecipitate (fig. S5B). Detection of radiolabeled uridine 5′-monophosphate (pU) in nuclease P1 digests of introns circularized by c-myc–HSPC117 but not by T4 Pnkp/Rnl1 supported retention of the splice junction phosphate (Fig. 2E, compare lanes 1 and 2). Therefore, HSPC117 joins tRNA exon halves by incorporating the precursor-derived splice junction phosphate into the mature tRNA as a canonical 3′,5′-phosphodiester, as previously shown (*12*, *13*).

In an unrelated effort aiming to purify spliceosomal particles, we discovered that a complex containing HSPC117 was co-selected during immunoaffinity chromatography of human SF3b complexes (fig. S6A). SF3b is essential for pre-mRNA splicing and associates with the U2 small nuclear ribonucleoprotein (snRNP). SF3b was affinity-selected from HeLa nuclear extract depleted of spliceosomal snRNPs. During size exclusion chromatography of the affinity-selected proteins, in addition to the SF3b complex (fractions 12 to 18), a smaller complex peaking in fractions 23 to 26 was observed (Fig. 3A, left panel). This complex contained HSPC117 together with the DEAD-box helicase DDX1, CGI-99/C14ORF166, FAM98B, and two forms of ASW/C2ORF49 (Fig. 3A, right panel, and table S2). This set of proteins overlaps with the MS analysis results of immunoprecipitates of c-myc–HSPC117 from stable cell clones (table S3) and the proteins identified in the MonoQ RNA>p ligase fraction (table S1). Consistent with a role of an HSPC117 complex in RNA ligation, we were able to inhibit interstrand ligation and tRNA maturation reactions by addition of DNA duplexes reported to specifically bind to HSPC117, DDX1, and CGI-99 (*24*) (fig. S9). Fractions containing the HSPC117 complex, but not the SF3b complex, were sufficient to convert tRNA exon halves and linear intron into mature tRNA and circularized intron (Fig. 3B) and were able to rescue the tRNA maturation defect upon depletion of HSPC117 in cell extracts (fig. S6B). Ligation by the HSPC117 complex was strongly stimulated by the addition of ATP (*25*) (fig. S7). Because efficient depletion of the HSPC117-interacting proteins did not compromise interstrand ligation or tRNA maturation as severely as did silencing of HSPC117 itself (Fig. 3, C to F, and fig. S8), and because mutation of a single, highly conserved cysteine residue of HSPC117 abolishes its RNA ligase activity (Fig. 2A and fig. S4), we conclude that HSPC117 is the only essential subunit of the ligase complex. It is noteworthy that the *Pyrobaculum aerophilum* RtcB protein was recently identified as a monomeric archaeal RNA>p ligase (*26*).

In living cells, interstrand ligation was dependent on HSPC117 (Fig. 4A, compare lanes 4 and 7 with lanes 3 and 6, respectively) and RNA 3′-P terminal cyclase (RTCD1) (Fig. 4A, compare lanes 5 and 8 with lanes 3 and 6, respectively). To test the effect of silencing of HSPC117 on processing of de novo synthesized pre-tRNA, we followed the fate of inducible pre-tRNA reporter transcripts in living cells. Induced transcription of intron-containing reporter pre-tRNAs distinguishable from endogenous pre-tRNAs (fig. S10A) revealed a delay in the formation of mature tRNA in cultured cells depleted of HSPC117 (Fig. 4B, compare lanes

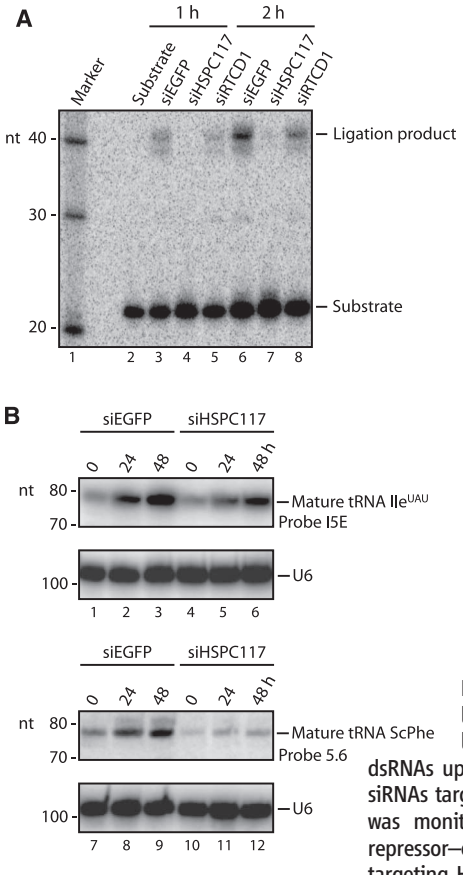

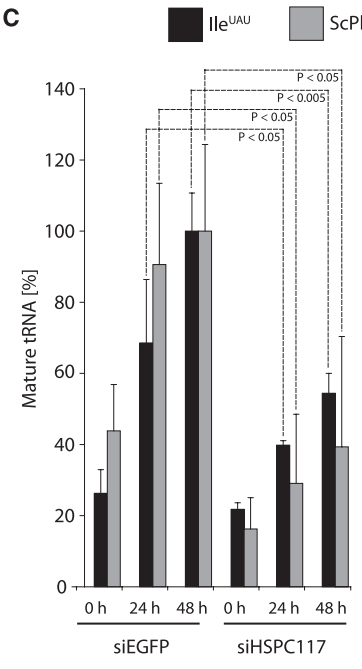

Fig. 4. Silencing of HSPC117 abolishes interstrand ligation and partially impairs tRNA processing in living cells. (**A**) Ligation of radiolabeled 3′-P, 5′-OH dsRNAs upon transfection into HeLa cells pretransfected with siRNAs targeting HSPC117, RTCD1, or EGFP as a control gene was monitored by denaturing gel electrophoresis. (**B**) Tet repressor–expressing HeLa cells were cotransfected with siRNAs targeting HSPC117 or EGFP and reporter constructs encoding Tet-inducible pre-tRNA Ile^{UAU} (lanes 1 to 6) or pre-tRNA ScPhe (lanes 7 to 12). After induction, RNA was isolated at indicated time points and analyzed by Northern blot. (**C**) The signals corresponding to mature tRNA were quantified by phosphorimaging. Values were normalized to U6 hybridization signals; the signals obtained in EGFP siRNA treated cells at 48 hours were arbitrarily set to 100%. Values are depicted as means ± SD; *P* values were obtained by unpaired *t* test (*N* = 3).

1 to 3 with lanes 4 to 6 and lanes 7 to 9 with lanes 10 to 12, and Fig. 4C). These data establish a role for HSPC117 as an RNA ligase with broad substrate specificity and with a function in tRNA processing in living cells.

Both RNA>p ligase and T4 Rnl1–like ligation mechanisms have been detected in human cells (*12*, *27*) but RNA>p ligase seems to play a dominant role in human tRNA splicing (*12*, *28*). We have identified HSPC117 as an essential component of the prevalent human tRNA splicing pathway. Recently, HSPC117 or the RNA>p ligase pathway have also been implicated in RNA processing during viral replication (*29*, *30*). The high degree of conservation of HSPC117/RtcB proteins is suggestive of shared roles for this protein family in organisms as distantly related as humans and *E. coli*.

References and Notes

1. E. M. Phizicky, A. K. Hopper, *Genes Dev.* **24**, 1832 (2010).
2. S. V. Paushkin, M. Patel, B. S. Furia, S. W. Peltz, C. R. Trotta, *Cell* **117**, 311 (2004).
3. C. R. Trotta *et al.*, *Cell* **89**, 849 (1997).
4. J. Abelson, C. R. Trotta, H. Li, *J. Biol. Chem.* **273**, 12685 (1998).
5. M. Englert, H. Beier, *Nucleic Acids Res.* **33**, 388 (2005).
6. M. Konarska, W. Filipowicz, H. Domdey, H. J. Gross, *Nature* **293**, 112 (1981).
7. E. M. Phizicky, R. C. Schwartz, J. Abelson, *J. Biol. Chem.* **261**, 2978 (1986).
8. L. K. Wang, C. K. Ho, Y. Pei, S. Shuman, *J. Biol. Chem.* **278**, 29454 (2003).
9. B. L. Apostol, S. K. Westaway, J. Abelson, C. L. Greer, *J. Biol. Chem.* **266**, 7445 (1991).
10. R. Sawaya, B. Schwer, S. Shuman, *J. Biol. Chem.* **278**, 43928 (2003).
11. W. Filipowicz, M. Konarska, H. J. Gross, A. J. Shatkin, *Nucleic Acids Res.* **11**, 1405 (1983).
12. W. Filipowicz, A. J. Shatkin, *Cell* **32**, 547 (1983).
13. F. A. Laski, A. Z. Fire, U. L. RajBhandary, P. A. Sharp, *J. Biol. Chem.* **258**, 11974 (1983).
14. L. Zofallova, Y. Guo, R. Gupta, *RNA* **6**, 1019 (2000).
15. J. Martinez, A. Patkaniowska, H. Urlaub, R. Lührmann, T. Tuschl, *Cell* **110**, 563 (2002).
16. See supporting material on *Science* Online.
17. O. Vicente, W. Filipowicz, *Eur. J. Biochem.* **176**, 431 (1988).
18. EBI InterPro database entry www.ebi.ac.uk/interpro/IEntry?ac=IPR001233.
19. P. Genschik, K. Drabikowski, W. Filipowicz, *J. Biol. Chem.* **273**, 25516 (1998).
20. M. Y. Galperin, E. V. Koonin, *Nucleic Acids Res.* **32**, 5452 (2004).
21. K. Goyal, S. C. Mande, *Proteins* **70**, 1206 (2008).
22. C. Okada, Y. Maegawa, M. Yao, I. Tanaka, *Proteins* **63**, 1119 (2006).
23. S. Weitzer, J. Martinez, *Nature* **447**, 222 (2007).
24. V. Drewett *et al.*, *Nucleic Acids Res.* **29**, 479 (2001).
25. K. K. Perkins, H. Furneaux, J. Hurwitz, *Proc. Natl. Acad. Sci. U.S.A.* **82**, 684 (1985).
26. M. Englert, K. Sheppard, A. Aslanian, J. R. Yates III, D. Söll, *Proc. Natl. Acad. Sci. U.S.A.* 10.1073/pnas.1018307108 (2011).
27. M. Zillmann, M. A. Gorovsky, E. M. Phizicky, *Mol. Cell. Biol.* **11**, 5410 (1991).
28. H. P. Harding *et al.*, *RNA* **14**, 225 (2008).
29. D. Cao, D. Haussecker, Y. Huang, M. A. Kay, *RNA* **15**, 1971 (2009).
30. C. E. Reid, D. W. Lazinski, *Proc. Natl. Acad. Sci. U.S.A.* **97**, 424 (2000).

31. We thank H. Beier, T. Biederer, T. Clausen, A. Meinhart, A. F. Nielsen, R. Schroeder, K. Sheppard, T. Tuschl, and S. Westermann for reagents and helpful discussions; and G. Heyne, O. Kuzyk, G. Schmauss, and G. Stengl for technical assistance; and H. Urlaub for MS analysis of HSPC117 complexes. M.E. was a Feodor-Lynen Postdoctoral Fellow of the Alexander von Humboldt Stiftung (Bonn, Germany). Supported by grants from the European Commission (EURASNET-518238) (R.L.), the Fonds zur Förderung der wissenschaftlichen Forschung (W1207 RNA Biologie) (J.P.), and the National Institute of General Medical Sciences (D.S.). J.M. would like to especially acknowledge the generous financial contribution and support by S.D. Prinz Max von und zu Liechtenstein.

Supporting Online Material

www.sciencemag.org/cgi/content/full/331/6018/760/DC1
Materials and Methods
Figs. S1 to S10
Tables S1 to S3
References

15 September 2010; accepted 7 January 2011
10.1126/science.1197847

Proteome Half-Life Dynamics in Living Human Cells

Eran Eden,*† Naama Geva-Zatorsky,* Irina Issaeva, Ariel Cohen, Erez Dekel, Tamar Danon, Lydia Cohen, Avi Mayo, Uri Alon†

Cells remove proteins by two processes: degradation and dilution due to cell growth. The balance between these basic processes is poorly understood. We addressed this by developing an accurate and noninvasive method for measuring protein half-lives, called "bleach-chase," that is applicable to fluorescently tagged proteins. Assaying 100 proteins in living human cancer cells showed half-lives that ranged between 45 minutes and 22.5 hours. A variety of stresses that stop cell division showed the same general effect: Long-lived proteins became longer-lived, whereas short-lived proteins remained largely unaffected. This effect is due to the relative strengths of degradation and dilution and suggests a mechanism for differential killing of rapidly growing cells by growth-arresting drugs. This approach opens a way to understand proteome half-life dynamics in living cells.

Protein removal plays a role in numerous cellular processes, including cell cycle regulation, differentiation, apoptosis, and signal transduction (*1*, *2*), and in disease (*3*, *4*). Understanding the principles that govern protein removal is needed to understand how cells regulate their proteome.

Cells remove proteins by two main processes: intracellular degradation (*2*) (e.g., via the proteasome) and dilution, which is due to cell growth, effectively reducing the protein amount by 50% with every division (*5*, *6*). Degradation can selectively regulate individual proteins, whereas changes in dilution rate globally affect the proteome. The balance between these two processes varies across organisms and cell types. In rapidly dividing cells, such as bacteria, dilution is often more dominant than degradation, and thus, growth-rate largely determines the protein removal rate (*6*, *7*). In contrast, nondividing and slowly dividing cells, such as differentiated mammalian cells, seem to rely mostly on degradation, because dilution is negligible. In mammalian cells that undergo moderate cell growth, including cancer cells, a systems-level understanding of the balance between these two fundamental processes is lacking.

Studying protein removal requires a method that should ideally: (i) facilitate measurements of many proteins, (ii) cause minimal interference to the cell, (iii) have high temporal resolution and accuracy, and (iv) work in living cells. A traditional method, "pulse-chase," radioactively labels the protein of interest over a brief period (the pulse), and then the decay in radioactivity is measured over time (the chase) and is used to infer protein half-life (*7*). This assay is accurate and minimally perturbative but requires a specific antibody for each protein and is difficult to scale to multiple proteins. One way to increase throughput is to integrate pulse-chase with mass spectrometry (*5*). However, this approach does not enable real-time monitoring of living cells. Protein synthesis inhibitors have also been used to measure removal rates but lead to severe cell perturbation. Another approach uses dual-fluorescent reporters to estimate relative protein turnover (*8*) but does not supply quantitative half-lives.

We present an assay called "bleach-chase" for measuring protein half-lives that does not require translation inhibitors, antibodies, or radioactive labeling. It can be applied to multiple proteins and time points in living cells and is generally applicable to fluorescently tagged proteins (Fig. 1A). We first provide a description of the idea behind bleach-chase and then turn to experimental tests of the method.

We use the term "degradation" to refer to intracellular processes that lead to proteolysis, such as lysosome- and proteasome-mediated degradation. Protein removal rate, α, is the sum of the degradation, α_{deg}, and the dilution rate, α_{dil} (*6*, *9*)

$$\alpha = \alpha_{deg} + \alpha_{dil} \quad (1)$$

In the bleach-chase method, the fluorophore of the tagged protein is bleached using a brief pulse

Department of Molecular Cell Biology, Weizmann Institute of Science, Rehovot 76100, Israel.

*These authors contributed equally to this work.
†To whom correspondence should be addressed. E-mail: eraneden@gmail.com (E.E.); urialon@weizmann.ac.il (U.A.)